Atmos. Chem. Phys. Discuss., 14, 25825–25867, 2014
www.atmos-chem-phys-discuss.net/14/25825/2014/
doi:10.5194/acpd-14-25825-2014

Atmospheric Chemistry and Physics Discussions

Characterization of satellite based proxies for estimating nucleation mode particles over South Africa

A.-M. Sundström[1], A. Nikandrova[1], K. Atlaskina[1], T. Nieminen[1], V. Vakkari[2,1], L. Laakso[2,3], J. P. Beukes[3], A. Arola[4], P. G. van Zyl[3], M. Josipovic[3], A. D. Venter[3], K. Jaars[3], J. J. Pienaar[3], S. Piketh[3], A. Wiedensohler[5], E. K. Chiloane[3,6], G. de Leeuw[2], and M. Kulmala[1]

[1]Department of Physics, University of Helsinki, Helsinki, Finland
[2]Finnish Meteorological Institute, Helsinki, Finland
[3]Unit for Environmental Science and Management, North-West University, Potchefstroom, South Africa
[4]Finnish Meteorological Institute, Kuopio, Finland
[5]Leibniz Institute for Tropospheric Research, Leipzig, Germany
[6]Eskom Holdigns SOC Ltd, Sustainability Division, South Africa

Received: 8 August 2014 – Accepted: 15 September 2014 – Published: 14 October 2014

Correspondence to: A.-M. Sundström (anu-maija.sundstrom@helsinki.fi)

Published by Copernicus Publications on behalf of the European Geosciences Union.

Abstract

In this work satellite observations from the NASA's A-Train constellation were used to derive the values of primary emission and regional nucleation proxies over South Africa to estimate the potential for new particle formation. As derived in Kulmala et al. (2011), the satellite based proxies consist of source terms (NO_2, SO_2 and UV-B radiation), and a sink term describing the pre-existing aerosols. The first goal of this work was to study in detail the use of satellite aerosol optical depth (AOD) as a substitute to the in situ based condensation sink (CS). One of the major factors affecting the agreement of CS and AOD was the elevated aerosol layers that increased the value of column integrated AOD but not affected the in situ CS. However, when the AOD in the proxy sink was replaced by an estimate from linear bivariate fit between AOD and CS, the agreement with the actual nucleation mode number concentration improved somewhat. The second goal of the work was to estimate how well the satellite based proxies can predict the potential for new particle formation. For each proxy the highest potential for new particle formation were observed over the Highveld industrial area, where the emissions were high but the sink due to pre-existing aerosols was relatively low. Best agreement between the satellite and in situ based proxies were obtained for NO_2/AOD and UV-B/AOD^2, whereas proxies including SO_2 in the source term had lower correlation. Even though the OMI SO_2 boundary layer product showed reasonable spatial pattern and detected the major sources over the study area, some of the known minor point sources were not detected. When defining the satellite proxies only for days when new particle formation event was observed, it was seen that for all the satellite based proxies the event day medians were higher than the entire measurement period median.

ACPD
14, 25825–25867, 2014

1 Introduction

Aerosol particles are key constituents in the Earth–Atmosphere system that can alter climate through their direct and indirect effects on Earth's radiation budget. Aerosols affect the radiation budget directly by scattering and absorbing solar radiation, and indirectly by acting as cloud condensation nuclei or ice nuclei and modifying clouds' radiative properties and lifetimes. However, the quantification of the aerosol effects on climate is very complex and large uncertainties still exist due to the high spatial and temporal variability of aerosol mass and particle number concentrations (e.g. IPCC, 2013). Besides the climatic effects, aerosols affect human life by reducing the air quality and visibility as well as affecting human health especially in urban areas. Particulate air pollution has been associated with adverse cardiovascular and pulmonary diseases, and even with rises in the numbers of deaths among older people (e.g. Seaton et al., 1995; Uttel et al., 2000; Schnelle-Kreis, 2009).

Primary aerosol particles are emitted directly to the atmosphere e.g. from biomass burning, fossil fuel combustion or re-suspended dust from disturbed or un-vegetated soil. Secondary particles are on the other hand nucleated via gas-to-particle conversion. The key phenomena associated with secondary atmospheric aerosol system are the formation of new nanometer-size aerosol particles and their subsequent growth to climatically relevant sizes ($D_p \sim 100$ nm), i.e. to sizes when their direct and indirect contribution to Earth's radiation budget becomes significant. The atmospheric aerosol formation is strongly connected to the formation of sulphuric acid and other vapours of very low volatility, as well as the magnitude of solar radiation (e.g. Kulmala et al., 2008, 2005). On the other hand pre-existing aerosol particles act as a sink for the vapours inhibiting new aerosol formation (e.g. Kulmala et al., 2008).

Several studies have shown that nucleation occurs frequently in the continental boundary layer and free troposphere from clean to polluted environments (Kulmala et al., 2004, 2008 and references therein). Laakso et al. (2008) and Vakkari et al. (2011) have studied new particle formation over moderately polluted savannah ecosystems in

ACPD
14, 25825–25867, 2014

South Africa and found that nucleation takes place in the boundary layer almost every sunny day throughout the year with a frequency as high as 69 % of all analyzed days (Vakkari et al., 2011). Hirsikko et al. (2012) extended the studies in South Africa to a polluted measurement site and found even higher frequency for the nucleation event days (86 %), which is among the highest event frequencies reported in the literature so far. Hirsikko et al. (2013) also studied the causes for two or three consecutive daytime nucleation events, followed by subsequent particle growth during the same day. They concluded e.g. that the multiple events were associated with SO_2 rich air from industrial sources.

Satellite instruments have been providing global observations of the Earth's atmosphere for three decades (e.g. Lee et al., 2009; Kokhanovsky and de Leeuw, 2009). Information about the spatial distribution of aerosols and trace gases can be obtained from multiple instruments with various temporal and spatial resolution and coverage. Passive remote sensing instruments such as NASA's Ozone Monitoring Instrument (OMI) onboard AURA platform or Moderate Resolution Imaging Spectroradiometer (MODIS) onboard Terra and Aqua platforms use the solar radiation to detect either trace gases or aerosol and cloud properties. The trace gas remote sensing techniques are based on the trace gas absorption features in the UV-region (wavelength $\lambda \sim 200$–400 nm), whereas the remote sensing of aerosol particles is mainly based on measurements in the visible and near infrared regions ($\lambda \sim 500$–2000 nm). Since the aerosol measurements utilizes only the optically active size range of the solar spectrum, the detectable aerosol sizes are limited to particles diameter greater than about 100 nm. Nucleation mode particles (smaller than about 25–30 nm in diameter), therefore, cannot be detected directly using the satellite instruments. In 2011, Kulmala et al. (2011) introduced proxies, i.e. satellite based parameterizations for estimating the concentrations of nucleated particles smaller than about 25–30 nm in diameter. Their study was the first attempt to estimate the global nucleation mode aerosol concentrations based on satellite measurements. The satellite proxies are defined as the ratio of the source and sink terms. The nucleation source terms consisted of trace gas column

ACPD
14, 25825–25867, 2014

densities (NO_2 or SO_2) and UV-radiation (from OMI) whereas the sink due to pre-existing aerosols was estimated using aerosol optical depth (AOD, from MODIS). More recently Crippa et al. (2013) formulated a new proxy algorithm for ultrafine particle number concentrations based on satellite-derived parameters. They used multivariate linear regression approach to derive the proxy, where the source terms consisted of SO_2, UV (from OMI), and NH_3 (from Tropospheric Emission Spectrometer, TES). The sink term was formulated using MODIS (collection 5.0) AOD and the Ångström coefficient, which expresses the spectral dependence of AOD on the wavelength. However, caution is needed if using the satellite-based Ångstrom coefficient especially over land. For MODIS collection 5 there have been reported issues with the Ångström coefficient (e.g. Mielonen et al., 2011), and thus it is not included anymore in the most recent MODIS collection 6.0 land parameters (Levy et al., 2013).

In this work the method introduced at Kulmala et al. (2011) is used to determine the satellite based proxies for estimating the potential for new particle formation over north-eastern part of South Africa (25–28° S, 25.5–30.5° E, Fig. 1.). Even though the study area is not very large, it comprises lots of contrasts from the emission point of view; the cities of Johannesburg and Pretoria, as well as highly industrialized areas especially east from the cities, and on the other hand very clean background in the western part of the study area. The study period considered in this paper was January 2007–December 2010. There are also four different measurement stations located within the region of interest, where observations of various in situ parameters were available. This work comprises of two parts:

1. A detailed investigation of using the satellite based AOD to describe the sink, and comparison with the in situ condensation sink (CS).

2. To estimate how well the satellite based proxies can predict the new particle formation over the study area. This comprises of the analysis of the satellite based proxy components and proxies, as well as the comparison with the in situ observations, including also the event classification data.

ACPD
14, 25825–25867, 2014

Even though the connection between the AOD and CS is very important, it has not been studied in detail before, starting from the theoretical definitions of the parameters and continuing to the comparison of the in situ and satellite based observations. Also, the satellite based proxies have not been extensively compared with in situ measurements, and especially with the new particle formation event classification data.

2 Data

In this study data from NASA's Afternoon-Train (A-Train) constellation was used. The A-Train constellation consists of seven satellites that are on a same polar-orbiting track and follow each other closely enabling near-simultaneous observations of variety of atmospheric parameters. The equatorial overpassing time for the A-Train satellites is around 1.30 p.m. In this study the OMI instrument aboard NASA's AURA satellite was used to get the NO_2 and SO_2 column densities as well as the amount of UV-B radiation. The measurement range of OMI covers spectral region from 264 to 504 nm, and the nominal spatial resolution is 13 km × 24 km. Global coverage is achieved in one day. For this study the selected Level 2 OMI parameters were NO_2 tropospheric column (Bucsela et al., 2013), the SO_2 planetary boundary layer (PBL) column product (Krotkov et al., 2006, 2008), and for UV-B the 310 nm irradiance at surface at local noon (Tanskanen et al., 2006). The OMI L2 parameters were gridded into 3 km × 3 km geographical grid and four year medians (2007–2010) were calculated as in Fioletov et al. (2011). In this way the effective spatial resolution could be increased despite the instrument resolution is coarser than the grid. For NO_2 and SO_2 only those observations were used where the (radiative) cloud fraction was below 20 %.

The AOD was obtained from MODIS onboard Aqua platform, which is measuring key aerosol and cloud properties in 36 spectral bands ranging from 0.4 to 14.0 µm. The spatial resolution of MODIS is 250–1000 m, depending on the measurement channel. The swath width is 2330 km, and global coverage is achieved in one day. In this study the recently released MODIS Aqua collection 6.0 AOD product at 3 km resolution was

ACPD
14, 25825–25867, 2014

used (Levy et al., 2013). For selected cases also data from The Cloud–Aerosol Lidar and Infrared Pathfinder Satellite Observation (CALIPSO) (Winker et al., 2007) were used to get the vertical profiles of aerosol extinction.

The in situ data were collected at four different stations in South Africa: Elandsfontein (ELA), Marikana (MAR), Botsalano (BOT), and Welgegund (WEL). All the stations are located in the north eastern part of the country (Fig. 1). Depending on the station, the measured parameters included e.g. particle size distribution, extinction coefficient and trace gas concentrations. More detailed descriptions of the in situ measurements can be found e.g. in Kulmala et al. (2011), Beukes et al. (2014), Hirsikko et al. (2012), Venter et al. (2012), Vakkari et al. (2011, 2013), and Laakso et al. (2012). Also data from the Aerosol Robotic Network (AERONET, http://aeronet.gsfc.nasa.gov, Holben et al., 1998) was used at Elandsfontein station. AERONET is a global ground-based sunphotometer network, providing observations of aerosol optical, microphysical, and radiative properties that are available in a public domain. The aerosol optical properties in the total atmospheric column are derived from the direct and diffuse solar radiation measured by the Cimel sunphotometers. Table 1 summarizes the data used in this work.

3 Proxies

Regional scale nucleation is associated with photochemistry, and typically has spatial scale of hundreds of kilometres (Kulmala et al., 2011, and references therein). The number concentration of nucleation mode particles on a regional scale can be estimated as a ratio of source term proportional to UV-radiation and sulphur dioxide concentration and a sink term (Petäjä et al., 2009):

$$P_{N_{\text{nuc, regional}}} = \frac{\text{UV}[\text{SO}_2]}{\text{CS}^2} \quad (1)$$

ACPD
14, 25825–25867, 2014

Primary emissions occur in the vicinity of local sources such as industrial or urban areas. For nucleation from primary emissions two proxies are defined as (Kulmala et al., 2011):

$$P_{N_{\text{nuc, prim.}}} = \frac{[NO_2]}{CS}, \quad (2)$$

$$P_{N_{\text{nuc, prim.}}} = \frac{[SO_2]}{CS}, \quad (3)$$

In each of the satellite-based proxies the source terms are estimated from the satellite measurements by replacing the SO_2 and NO_2 concentrations at the surface with the total column densities from the satellite. The amount of global UV radiation is also available from satellite measurements e.g. as a local noon irradiance at surface at 310 nm wavelength (UV-B-radiation). On the other hand for the sink term there is no equivalent column integrated parameter from satellites. For satellite based sink parameter Kulmala et al. (2011) proposed aerosol optical depth (AOD) that describes the total aerosol extinction in an atmospheric column. The relation between actual CS and AOD will be discussed in more detail in the following section. By replacing CS with AOD the satellite based proxies can be expressed for primary nucleation as

$$P^{\text{Sat.}}_{N_{\text{nuc}}} = \frac{[NO_2]_{\text{column}}}{AOD} \quad (4)$$

$$P^{\text{Sat.}}_{N_{\text{nuc}}} = \frac{[SO_2]_{\text{column}}}{AOD}, \quad (5)$$

and for regional nucleation as

$$P^{\text{Sat.}}_{N_{\text{nuc}}} = \frac{UV[SO_2]_{\text{column}}}{AOD^2} \quad (6)$$

In addition we also considered

$$P^{\text{Sat.}}_{N_{\text{nuc}}} = \frac{UV}{AOD^2} \quad (7)$$

ACPD
14, 25825–25867, 2014

as a potential proxy for the number concentration of nucleation mode particles.

3.1 Condensation sink and aerosol extinction

As indicated in the previous section, Kulmala et al. (2011) proposed AOD as a substitute for CS. Both parameters are also roughly proportional to the aerosol surface area distribution. According to e.g. Lehtinen et al. (2003) the condensation sink is defined as

$$\mathrm{CS} = 2\pi\rho_{\mathrm{diff}} \int_0^\infty D_{\mathrm{p}}\beta_{\mathrm{M}}(D_{\mathrm{p}})n(D_{\mathrm{p}})\mathrm{d}D_{\mathrm{p}}, \quad (8)$$

where D_{p} is the particle radius, $n(D_{\mathrm{p}})$ is the particle number size distribution function, ρ_{diff} is the diffusion coefficient, and $\beta_{\mathrm{M}}(D_{\mathrm{p}})$ is the transitional correction factor.

Aerosol optical depth describes quantitatively the column-integrated extinction of solar light caused by atmospheric aerosols and it is one of the standard aerosol parameters that is retrieved from the satellite radiance observations. At some constant height z and wavelength λ the aerosol extinction is defined as

$$\sigma_{\mathrm{ext}}(z,\lambda) = \frac{1}{4}\pi \int_0^\infty Q_{\mathrm{ext}}(\lambda, D_{\mathrm{p}}, m)D_{\mathrm{p}}^2 n(D_{\mathrm{p}})\mathrm{d}D_{\mathrm{p}}, \quad (9)$$

where Q_{ext} is the extinction efficiency describing aerosols ability to scatter and absorb solar light. At fixed wavelength the extinction efficiency is a complex function of aerosol size and complex refractive index m (composition). Also the particles shape affects somewhat on Q_{ext}, but this is not considered in this study. If the particles are assumed to be spherical, Q_{ext} can be calculated using a computer code based on the Lorenz–Mie theory (Mishchenko et al., 2002). AOD is obtained by integrating σ_{ext} over the total atmospheric column.

ACPD
14, 25825–25867, 2014

If the satellite retrievals provided the aerosol size distribution, CS could be derived from the satellite observations. Since this is not the case, the sink of existing aerosols is estimated using the column integrated value of σ_{ext}, i.e. AOD. Figure 2 illustrates the theoretical differences between CS and σ_{ext} (at a constant atmospheric level) as a function of particle size. Both parameters are derived using the same aerosol size distribution (Fig. 2, left panel). The σ_{ext} is calculated using a refractive index of $m = 1.48 + 0.003i$ and wavelengths of 0.55 and 0.45 µm. As Fig. 2 shows, particles with D_p about 0.05–0.1 µm have the largest contribution to CS, whereas for σ_{ext} the largest contribution is coming from particles with D_p about 0.2–0.8 µm. The notable difference between the two quantities is that particles $D_p < 0.1$ µm can have several orders of magnitude larger contribution to CS than σ_{ext}. On the other hand, σ_{ext} is significantly more sensitive to the particles with $D_p > 1.0$ µm than CS. It is clear that e.g. a large change in number concentration of the smaller particle sizes would change the value of total CS when integrated over the size distribution, but would have only a minor effect on the value of σ_{ext}, and vice versa, if e.g. the number concentration of large particles increased. It is noted that in addition to the theoretical differences the possibility of elevated aerosol layers affect the column integrated values of σ_{ext}, i.e. the AOD, which must be considered when comparing the satellite based AOD with in situ CS.

The sensitivity of σ_{ext} on particle sizes depends to a certain extent on the particle composition and the measurement wavelength. If absorption is significantly high (i.e. the imaginary part of $m \sim 0.1i$), the contribution of particles $D_p < 0.1$ µm to σ_{ext} would be somewhat higher than in Fig. 2. Shorter wavelengths increase the sensitivity to smaller particles, but as Fig. 2 illustrates, a 0.1 µm decrease in wavelength does not improve the sensitivity significantly. Much shorter wavelengths would be needed to increase the sensitivity of σ_{ext} to particles $D_p < 0.1$ µm, but such measurements could not be carried out in a real atmosphere.

ACPD
14, 25825–25867, 2014

4 Results

4.1 Comparison of condensation sink and aerosol optical depth

Replacing CS with AOD is perhaps the most crucial assumption when determining the proxies using satellite data, as indicated in Kulmala et al. (2011). The theoretical differences between aerosol extinction and CS are illustrated in Fig. 2, but when comparing satellite AOD with CS other issues might arise related to for example, the in situ measurement devices and aerosol vertical distribution. CS is determined from the measured dry particle size distribution with a correction for ambient humidity. At Botsalano and Marikana CS has been estimated from submicron size distribution up to 10 µm was used. On the other hand, as the AOD is an integrated quantity through the total atmospheric column, it has contribution from all optically active aerosols at all atmospheric levels. To assess the effect of these different factors on the relation between the AOD and CS the following comparisons were carried out:

1. in situ CS and nephelometer aerosol scattering coefficient;
2. in situ nephelometer aerosol scattering coefficient and column integrated AOD from AERONET;
3. in situ CS and column integrated aerosol extinction from both AERONET- and satellite measurements.

Coincident measurements of situ size distributions to derive the CS and in situ scattering from nephelometer were only available at Elandsfontein measurement station. The comparison between CS and scattering coefficient was intended to mainly illustrate the theoretical differences in CS and aerosol extinction because both measurements were carried out at ground level and elevated aerosol layers would not affect the comparison. The nephelometer measures the dry particle scattering at 0.525 µm wavelength. The results are presented at a Standard Temperature and Pressure (STP) atmosphere, and the maximum particle size was limited to a $D_p \sim 10$ µm. It should be

ACPD
14, 25825–25867, 2014

noted that the nephelometer considers only aerosol scattering, and not the total extinction which would also require the information about absorption. However, the contribution of absorption to total aerosol extinction is generally much smaller than scattering. Laakso et al. (2012) reported that at Elandsfontein the absorption was increased during the coldest months (May–October) due to the biomass burning season and domestic burning of coal for heating as well as cooking, contributing about 15–20 % of the total aerosol extinction whereas during the warmer months (November–April) absorption contributed ~ 10 % of the total aerosol extinction. Due to the seasonal variation of absorption, the comparison between one hour mean CS and scattering coefficient was carried out separately for May–October and November–April. For both periods significant correlations between in situ scattering and CS were found: 0.82 ($p < 0.001$) for November–April, and 0.84 ($p < 0.001$) for May–October (Fig. 3). The correlations were higher than what has been reported at clean continental boreal forest measurement site in Hyytiälä, Southern Finland, by Virkkula et al. (2011). They obtained a correlation coefficient of 0.62 between CS and the scattering coefficient.

The next step was to compare the nephelometer scattering coefficient to the column integrated aerosol extinction to find out how much the possible elevated aerosol layers and/or boundary layer mixing might affect the comparison. Also the presence of large dust particles might have some effect on the comparison due to the limited particle size in the nephelometer inlet. As Fig. 4 shows, lower correlations were obtained between column integrated AERONET AOD and in situ scattering coefficient (correlation coefficient warm season; 0.68, cold season; 0.49) than what were obtained between the in situ CS and scattering coefficient. This indicates that the elevated aerosol layers and boundary layer mixing might affect more than the theoretical differences when estimating the sink of pre-existing aerosols by using the AOD.

Finally the in situ CS was compared with the MODIS AOD. The daily AOD values used in the comparison were the spatial averages calculated from the observations within 3 km radius around the measurement station. As Fig. 5 shows, the CS-satellite AOD data were scattered and correlation was lower than in the previous comparisons

ACPD
14, 25825–25867, 2014

in Figs. 3 and 4, varying between 0.17 and 0.25 depending on the location. In addition, the standard least-squares method (LSQ) did not seem to give a proper slope for the coincident CS and AOD values. Therefore a bivariate method by York et al. (2004) was applied that accounts the uncertainties associated to both CSs and MODIS AODs in the fitting. For CS the uncertainty was assumed to be 10 %, which should be a reasonable estimate referring to the work by Petäjä et al. (2013). For MODIS AOD an uncertainty of 0.05 + 15 % was used as suggested in Levy et al. (2013). As Fig. 5 shows the bivariate method gave very different slopes than LSQ at each station for the relationship between CS and AOD, which might be partly related to the differences in the size distribution upper limits at Elandsfontein and Marikana/Botsalano. If the coincident CS-AOD observations at all three stations were combined, the bivariate fit gives $y = 0.194x - 0.008$.

At Marikana and Elandsfontein the largest observed AODs were not related to lagest CS, which could indicate the presence of elevated aerosol layers. At Marikana the median MODIS AOD was 0.15 for the whole measurement period, and as Fig. 5 shows, the CS values were less scattered when AODs were below the median. Also the correlation coefficient for coincident CS and AOD ≤ 0.15 was higher ($R = 0.4$, $p < 0.001$) than for the whole range of observations. To estimate how much the elevated aerosol layers might affect the CS-AOD comparison, CALIPSO observations of aerosol vertical extinction profiles were studied. All the CALIPSO daytime overpasses between 8 February 2008 and 17 May 2010 within 50 km from the Marikana station were considered. Since the CALIPSO swath width is narrow only 48 days of data were obtained. The vertical aerosol extinction profiles from CALIPSO were studied separately for the cases where MODIS AOD ≤ 0.15 and AOD > 0.15. As Fig. 6 shows, for higher AODs the median extinction profile indicated an elevated aerosol layer, which supports the result that high AODs at Marikana are likely to be associated with an elevated aerosol layer.

ACPD
14, 25825–25867, 2014

4.2 Spatial and seasonal characterization of the satellite proxy components

Each of the satellite based parameter was analyzed from January 2007 to December 2010. Figure 7 shows the four year medians of SO_2 and NO_2 column densities obtained from the OMI measurements, as well as the AOD at 550 nm from MODIS Aqua observations. The NO_2 and SO_2 column medians are calculated from data, where more than 80 % of the photons originate from the cloud-free area of the pixel, whereas the AOD represents only cloud-free cases. The clear sky noon UV-B irradiance depends on the season and hence has only small spatial variation at the time of the satellite overpass during the year. Highest amount of UV-B radiation is obtained naturally during summer (December–February), and lowest during winter (June–August).

The use of long time series and fine 3 km × 3 km spatial grid reveals OMI "sub-pixel" spatial patterns from the satellite data. Some similarities in the distribution of the NO_2 and SO_2 column densities could be observed. Both parameters showed the highest median values over the Highveld Mpumalanga industrial area east from Johannesburg and Pretoria (around the Elandsfontein measurement station), where most of South Africa's coal-fired power station, as well as some metallurgical smelters and a large petrochemical plant are situated (Lourens et al., 2011). None of these large point sources currently apply de-SO_x or de-NO_x technology. For NO_2 the maximum median values south of Elandsfontein were about 10 times larger than over the background areas in the west of the study area. Elevated values for the NO_2 column density were also observed over Johannesburg as was previously indicated by Lourens et al. (2012) as well as over the Vereening area where another large coal-fired power station, numerous petrochemical operations and various metal smelters are located. The maximum medians for SO_2 PBL column densities (about 2.5 DU) were observed over area with several metallurgical smelters, North West from Elandsfontein. A local hotspot of SO_2 was also observed over the Vereening area. However, in contrast to the NO_2 values, the SO_2 column densities over Johannesburg were not notably higher than over the background areas. Overall the SO_2 column densities outside the two clear hotspots

ACPD
14, 25825–25867, 2014

had little variation, which is different to the spatial pattern of greenhouse gas emission inventory data shown in Vakkari et al. (2011). It seems that the satellite data is unable to detect some of the weaker well known SO_2 sources e.g. over the Rustenburg area. As Fig. 7 illustrates the spatial pattern for AOD was different from the other two parameters. Overall the four-year median AOD was low (approximately 0.1) over the major part of the study area. Highest medians (approximately 0.25) were observed over Johannesburg and Pretoria area, but somewhat elevated values were also observed over Rustenburg region that closely resembled the shape of the southern portion of the western Bushveld Igneous Complex (wBIC) geological deposit. Nine ferrochromium, platinum and base metal smelters occur within a 40 km radius within this southern part of the wBIC. Each of these smelters is loaded with ores from at least two different mines operating within the wBIC. A similar concentration of smelters also occurs in the area coinciding with the northern part of the SO_2 hotspot identified over the Mpumalanga Highveld (Fig. 7c). However, these smelters in the Mpumalanga Highveld are fed with ores that are not mined in their immediate vicinity. From the difference observed in AOD between these two areas with high metal smelter densities it can be deduced that the higher AOD measured in the area near Rustenburg is due to larger particles being emitted from mining activities. All the smelters in South Africa apply bag filter or wet venturi scrubbing to remove particulate matter, therefore the smelters do not make significant contributions to the AOD. All the coal-fired power stations and petrochemical operations also apply off-gas cleaning technologies, and hence relatively low four-year AOD medians (approximately 0.1–0.15) were also observed over the heavily industrialized Mpumalanga Highveld area where the highest NO_2 and SO_2 column densities were observed.

Figure 8 illustrates the seasonal anomalies (season median – four-year median) of NO_2, SO_2 and AOD. Overall it seems that the NO_2 and SO_2 have somewhat similar seasonal variation, but over Highveld they seem to have opposite anomalies during winter and summer. AOD also varies in a different phase. One of the major factor affecting the trace gas and AOD seasonal variation is the large scale biomass burning

ACPD
14, 25825–25867, 2014

season between June and September–mid-October, which e.g. causes the NO_2 column peak during winter (JJA) over the major part of the study area. During winter months an anti-cyclonic flow pattern dominates the Highveld area and the pollutants are re-circulated, resulting in a build-up of pollutants originating from all sources. In addition, domestic burning of coal for heating contributes to the increase of primary pollutants while prevailing stable meteorological conditions as well as the lack of precipitation enhances the effect (Laakso et al., 2012, and references therein).

The AOD values increased significantly during spring (SON). The later peak of AODs is likely to be partly related to the long range transported aerosols from the large scale biomass burning in southern Africa. Maritz et al. (2014) indicated that the peak in biomass burning within an approximate 1000 km radius around the study area considered in this paper is in September. The large scale fires intensify during June–August in central Africa and shift southward during spring. It is also seen recognisable how the NO_2 anomaly decreases over the northern part of Mpumalanga and the Johannesburg–Pretoria areas as the anti-cyclonic transport of pollutants weakens.

During summer the humidity is relatively high and it forms part of the rainy season in the studied region. Wet deposition of pollutants is therefore more efficient than during the dry season (May–October). Therefore the lowest column densities of NO_2 are observed between December and February. Also SO_2 column densities are generally lower than the four years median during summer. However, over Mpumalanga and the eastern part of Gauteng an increase was observed. During summer the AOD is still larger than the four year median. This might partly be explained by the prevalent wet and cloudy meteorological conditions that can affect the sampling and quality of the AOD data. During Autumn (March–May) the NO_2 and SO_2 column densities increase over Gauteng and western Mpumalanga.

4.3 Comparison of the satellite data and in situ measurements

In order to evaluate how well the satellite based proxies actually can describe the potential for new particle formation in the boundary layer, a number of comparisons with

ACPD
14, 25825–25867, 2014

the in situ data were carried out. The satellite data for each station was collected within a 12 km (NO_2, SO_2, UV-B) or a 3 km (AOD) radius from the station location. The in situ data were hourly means extracted between 13:00–14:00 LT, i.e. ±30 min within the approximate A-Train satellites overpass time. In Sect. 4.1 it was shown that in some cases the sink of pre-existing aerosols within the boundary layer could be overestimated when using AOD as a substitute to CS due to elevated aerosol layers. However, when the satellite based source terms were compared with the in situ data, significant correlations were found between the satellite NO_2 column densities and the in situ NO_x-NO as well as the satellite UV-B irradiance and the in situ global radiation at each measurement station. The highest correlation for NO_2 were obtained at Marikana ($R = 0.72$, $p < 0.001$), and lowest at Elandsfontein ($R = 0.51$, $p < 0.001$). For UV-B and global radiation the correlations were between 0.78–0.88 ($p < 0.001$). In Kulmala et al. (2011) the satellite based SO_2 was not included in the proxy analysis because the quality of the data was poor. In this study the middle-troposphere SO_2 data was replaced by the OMI boundary layer product (Sect. 3), which significantly improved the quality of the data and the spatial variation thereof (Fig. 7). However, for all the stations lower correlation between the satellite and in situ based SO_2 measurements were obtained than for the other source parameters. The highest correlation was obtained at Welgegund ($R = 0.47$, $p = 0.002$), but at Marikana there was practically no correlation at all ($R = 0.1$, $p = 0.16$) which indicates that the satellite is not able to present the SO_2 sources over the Rustenburg area as already discussed in Sect. 4.2.

4.4 Satellite based proxies

The proxies for primary emissions and regional nucleation were defined for each season between 2007 and 2010 using the equations introduced in Sect. 2. Figure 9 shows the four year median spatial pattern for the satellite based proxies. The highest potential for primary and regional nucleation was found over the Highveld industrial area, where the values of NO_2 and SO_2 columns were high but the sink (AOD) was low. For the NO_2/AOD proxy also elevated values were observed over the Johannesburg–

ACPD
14, 25825–25867, 2014

Pretoria area while the other proxies showed local minimum over these cities. Even though the wBIC is one of the major pyrometallurgical complexes in South Africa, the observed proxy values were low when compared to values over Highveld industrial area. The SO_2 related proxies and UV-B/AOD^2 even showed local minima over the Marikana–Rustenburg area, due to the higher AOD values (Fig. 7a).

The proxy values from both satellite observations and in situ measurements were defined for Elandsfontein, Botsalano, and Marikana measurement stations. The correlation between the satellite and the in situ proxies were calculated after converting the proxy values into log-scale (Table 2). A relatively high correlation for the NO_2/AOD proxy was obtained for Marikana and Elandsfontein, but at Botsalano the agreement was weak. This might be partly related to the low number ($N = 9$) of coincident satellite and in situ proxy observations. In addition the satellite AOD was extremely low at Botsalano (about 0.05), and it varied relatively more than the CS values, which resulted in stronger satellite proxy variation. This indicated that the satellite based proxies might show too high variability (noise) over background areas where the AOD is very low and close to the satellite detection limits. Also the UV-B/AOD^2 showed reasonable correlation with the in situ data while the correlation for the SO_2 related proxies was rather low at all of the stations. This was expected because of the relatively low correlation between the satellite and in situ SO_2.

The satellite proxy values were also compared with the actual number concentration of nucleation mode particles (N_{nuc}, $D_p < 30$ nm) at stations where the DMPS measurements were available. Figure 10 presents the comparison of satellite based NO_2/AOD and N_{nuc} at the Marikana station, where the number of coincident satellite proxy and number concentration observations were the highest. The correlation ($R = 0.31$, $p < 0.001$) was higher than for the other satellite based proxies, for which there were practically no correlation at all (Table 3). At Welgegund and Botsalano all the correlations with the nucleation mode number concentrations and satellite proxies were below 0.1.

ACPD
14, 25825–25867, 2014

To test if the correlation between N_{nuc} and satellite based proxies could be improved, AOD was replaced with a sink estimate obtained from the York method CS-AOD linear fit (Sect. 4.1). Even though some improvement in the correlations between satellite based proxies and N_{nuc} were obtained at Marikana station (Table 3), the correlations remained overall rather low.

4.5 Satellite based proxies and event day classification

The event day classification scheme by dal Maso et al. (2005) divides days into three main categories; event, undefined, and non-event days, based on the investigation of particle size distribution measurements. The event days can be further categorized into different sub-classes. The nucleation event classification was available at Marikana, Botsalano and Welgegund measurement stations. The event classification data was used to define the satellite based proxies at the station and the surroundings based on the stations event and non-event days. Unfortunately there were no temporally overlapping event classification data for the three stations, and hence the study was made separately for each station. As already showed in Vakkari et al. (2013) and Hirsikko et al. (2012), the nucleation event frequency is very high in South Africa. Table 2 summarizes the number of event- and non event days defined at the three stations between January 2007 and December 2010. In this study the different event subclasses were not considered, and the days were only classified as event, non-event, and undefined. Also, the satellite data were not considered from those days when the event classification was not available at the station.

In an event day N_{nuc} is high, and hence, it is also expected that the satellite proxy values should be elevated. As Table 4 shows, the difference between the number of event and non-event days was significant at the measurement stations, e.g. at Marikana only two days were classified as non-event during the study period. When considering the satellite based proxies at the stations it was found that all the non-event days were cloudy, and hence the satellite based proxies could not be determined for those days at the stations. Also event and undefined days consisted some cloudy days, but there

ACPD
14, 25825–25867, 2014

were also days when satellite data were available. In the majority of the cases when the proxy values could not be determined, the reason was that the MODIS cloud screen procedure had declared pixels cloudy and hence the AOD was missing. Figure 11 illustrates the satellite proxy medians, and differences between the event and non-event days based on the event classification carried out at Marikana station. For event days slightly higher proxy medians were observed at Marikana, even though non-event proxies did not have any contribution to the whole measurement period median. More pronounced positive event day proxy anomalies were seen on the south side of the station. For non-event days lower median values were observed over the cloud-free areas where the proxies could be determined. Nearest non-event day observations were about 45 km to the west of Marikana. It is noted that these differences between the measurement period and event day medians were detected only when looking data over longer time period. Based on the daily values of the satellite proxies it was not possible to define whether there was an event at the station or not. At least some non-event day data from the satellites would have been needed to study the differences on a daily basis between events and non-events.

The OMI UV-B irradiance at surface was the only satellite based data included in the proxies that could be obtained for both cloudy and cloud-free days. From the OMI irradiance retrievals it is also possible to define a cloud modification factor (CMF) which is the ratio of observed UV-B irradiance and modelled clear-sky UV-B irradiance at the surface. In practice CMF describes how much cloudiness alters the UV-B radiation that reaches the surface. On cloud-free days CMF = 1.0, but on cloudy and overcast days CMF values decrease depending on the spatial cloud coverage and thickness of the cloud deck. Since UV-B radiation plays a central role in new particle formation events (e.g. Hirsikko et al., 2012; Petäjä et al., 2009), CMF was retrieved for Marikana and Botsalano stations and divided into three classes according to the event classification data. Figure 12 illustrates the distribution of CMF in event, undefined, and non-event days. In each of the three classes the CMF was most often between 0.95 and 1.0 indicating either clear skies or some scattered cumulus clouds. This CMF data indicated

ACPD
14, 25825–25867, 2014

that during non-event days the proportion of CMF < 0.7 might be slightly higher than in the two other categories. However, it should be noted that the number of CMF observations between event and non-event days differed considerably (768 vs. 20) which explains e.g. the gaps in the non-event CMF distribution.

5 Conclusions

Four different satellite based proxies for estimating the number concentrations of nucleation mode particles and the potential for new particle formation were derived over South Africa. A distinct improvement in the quality of the proxy components was obtained when different satellite products were selected to those utilized by Kulmala et al. (2011). The recently released MODIS coll. 6 AOD product at 3 km × 3 km spatial resolution revealed small scale AOD variation that could not be observed when using coarser spatial grid. This was especially important when considering this study area, where the AOD is generally low (0.05–0.1). The four year medians of the OMI data (NO_2, SO_2, and UV-B) were also calculated in a 3 km × 3 km grid using the method of Fioletov et al. (2011), which also revealed "sub-pixel" features in the spatial pattern. Even though the OMI SO_2 product was changed to a planetary boundary layer data set and the spatial pattern generally improved, the satellite data still seemed to miss some of the well known smaller scale sources within the study area.

Kulmala et al. (2011) emphasized that the most crucial assumption in deriving the satellite based proxies was the replacement of the CS with AOD. Overall the AOD was near the satellite detection limits in many locations, which might result in "artificially" high values of the satellite based proxies. Despite the theoretical differences between CS and AOD, good correlation was obtained between in situ scattering and CS, but significantly lower correlations were obtained when the in situ scattering or CS were compared with aerosol extinction integrated over the total atmospheric column, i.e. AOD. One of the most probable reasons was the elevated aerosol layers, which were often related to the increased AOD values. When the other satellite based proxy com-

ACPD
14, 25825–25867, 2014

ponents were compared with the in situ data, the SO_2 column densities did not show that good agreement compared to the correlation with the NO_2 column density and the radiation. This was also observed when comparing the in situ and satellite based proxies – the highest correlations were obtained for NO_2/AOD and UV-B/AOD^2. When the satellite based proxies were compared with actual nucleation mode number concentrations the correlations were low ($0.06 \leq R \leq 0.31$). Some improvement, however, was obtained ($0.21 \leq R \leq 0.34$) when the AOD was replaced by the estimated sink from the York fit (Fig. 5).

South Africa is a challenging area to study the satellite proxies within, since the nucleation event frequency is very high. Generally the CS is very low and not very high source species is needed for an event to occur. During the study period (January 2007–December 2010) only few days were classified as non-event at the measurement stations. In addition all the non-event days were cloudy and the satellite proxies could not be determined. Despite of this, for each satellite based proxy a difference was seen between the entire measurement period median (namely event and unclear days) and event day median. At each measurement station where the event classification data was available the event day satellite proxy medians were larger than the entire measurement period median. From a single day satellite proxy values it was not possible to define whether there was an event or not.

In general this study showed that the satellite based proxies seem to be able to show the potential for nucleation events in a statistical sense. Actual data from non-event days would have been needed to carry out such study. More studies of the satellite based proxies in different type of locations and environments are needed to improve the proxies, and especially the sink term, further. The next step is to study the satellite based proxy approach in China, where, in addition to the elevated NO_2 and SO_2 column densities, the AOD signal is also strong.

Acknowledgements. This work is supported by Academy of Finland (1251427, 1139656, Finnish Centre of Excellence in Atmospheric Science 272041), European Research Council (ATMNUCLE) and The European Integrated project on Aerosol Cloud Climate and Air Qual-

ACPD
14, 25825–25867, 2014

ity Interactions (EUCAARI). Eskom and Sasol supplied logistical support for measurements at Elandsfontein, while the town council of Rustenburg supplied support to the measurement at Marikana. The OMI NO_2, SO_2 and UV data were obtained from the NASA Mirador service maintained by Goddard Earth Sciences Data and Information Services Center (GES DISC). The OMI surface UV data were obtained from the NASA Aura Validation Data Center (AVDC). The MODIS Aqua data were provided by NASA LAADS Web, and the CALIPSO data was obtained from NASA Atmospheric Science Data Center (ASDC).

References

Beukes, P., Vakkari, V., van Zyl, P. G., Venter, A., Josipovic, M., Jaars, K., Tiitta, P., Kulmala, M., Worsnop, D., Pienaar, J., Virkkula, A., and Laakso L.: Source region plume characterisation of the interior of South Africa, as measured at Welgegund, Clean Air Journal, 23, 7–10, 2013.

Bucsela, E. J., Krotkov, N. A., Celarier, E. A., Lamsal, L. N., Swartz, W. H., Bhartia, P. K., Boersma, K. F., Veefkind, J. P., Gleason, J. F., and Pickering, K. E.: A new stratospheric and tropospheric NO_2 retrieval algorithm for nadir-viewing satellite instruments: applications to OMI, Atmos. Meas. Tech., 6, 2607–2626, doi:10.5194/amt-6-2607-2013, 2013.

Crippa, P., Spracklen, D., and Pryor, S. C.: Satellite-derived estimates of ultrafine particle concentrations over Eastern North America, J. Geophys. Res., 118, 9968–9981, 2013.

Dal Maso, M., Kulmala, M., Riipinen, I., Wagner, R., Hussein, T., Aalto, P. P., and Lehtinen, K. E. J.: Formation and growth of fresh atmospheric aerosols: eight years of aerosol size distribution data from SMEAR II, Hyytiälä, Finland, Boreal Environ. Res., 10, 323–336, 2005.

Fioletov, V. E., McLinden, C. A., Krotkov, N., Moran, M. D., and Yang, K.: Estimation of SO_2 emissions using OMI retrievals, Geophys. Res. Lett., 38, L21811, doi:10.1029/2011GL049402, 2011.

Hirsikko, A., Vakkari, V., Tiitta, P., Manninen, H. E., Gagné, S., Laakso, H., Kulmala, M., Mirme, A., Mirme, S., Mabaso, D., Beukes, J. P., and Laakso, L.: Characterisation of submicron particle number concentrations and formation events in the western Bushveld Igneous Complex, South Africa, Atmos. Chem. Phys., 12, 3951–3967, doi:10.5194/acp-12-3951-2012, 2012.

ACPD
14, 25825–25867, 2014

Hirsikko, A., Vakkari, V., Tiitta, P., Hatakka, J., Kerminen, V.-M., Sundström, A.-M., Beukes, J. P., Manninen, H. E., Kulmala, M., and Laakso, L.: Multiple daytime nucleation events in semi-clean savannah and industrial environments in South Africa: analysis based on observations, Atmos. Chem. Phys., 13, 5523–5532, doi:10.5194/acp-13-5523-2013, 2013.

Holben, B., Eck, T. F., Slutsker, I., Tanre, D., Buis, J. P., Setzer, A., Vermote, E., Reagan, J. A., Kaufman, Y. J., Nakajima, T., Lavenu, F., Jankowiak, I., and Smirnov, A.: AERONET – a federated instrument network and data archive for aerosol characterization, Remote Sens. Environ., 66, 1–16, 1998.

IPCC, Intergovernmental Panel on Climate Change, Fifth Assessment Report: Climate Change, Cambridge University Press, Cambridge, UK and New York, NY, USA, 2013.

Kokhanovsky, A. A. and de Leeuw, G. (Eds.): Satellite Aerosol Remote Sensing over Land, Springer, Berlin, Germany, 2009.

Krotkov, N., Carn, S., Krueger, A., Bhartia, P., and Yang, K.: Band residual difference algorithm for retrieval of SO_2 from the Aura Ozone Monitoring Instrument (OMI), IEEE T. Geosci. Remote, 44, 1259–1266, 2006.

Krotkov, N., McClure, B., Dickerson, R., Carn, S., Li, C., Bhartia, P., Yang, K., Krueger, A., Li, Z., Levelt, P., Chen, H., Wang, P., and Lu, D.: Validation of SO_2 retrievals from the Ozone Monitoring Instrument over NE China, J. Geophys. Res., 113, D16S40, doi:10.1029/2007JD008818, 2008.

Kulmala, M. and Kerminen, V.-M.: On the formation and growth of atmospheric nanoparticles, Atmos. Res., 90, 132–150, 2008.

Kulmala, M., Vehkamäki, H., Petäjä, T., Dal Maso, M., Lauri, A., Kerminen, V.-M., Birmili, W., and McMurry, P. H.: Formation and growth rates of ultrafine atmospheric particles: a review of observations, J. Aerosol Sci., 35, 143–176, 2004.

Kulmala, M., Petäjä, T., Mönkkönen, P., Koponen, I. K., Dal Maso, M., Aalto, P. P., Lehtinen, K. E. J., and Kerminen, V.-M.: On the growth of nucleation mode particles: source rates of condensable vapor in polluted and clean environments, Atmos. Chem. Phys., 5, 409–416, doi:10.5194/acp-5-409-2005, 2005.

Kulmala, M., Arola, A., Nieminen, T., Riuttanen, L., Sogacheva, L., de Leeuw, G., Kerminen, V.-M., and Lehtinen, K. E. J.: The first estimates of global nucleation mode aerosol concentrations based on satellite measurements, Atmos. Chem. Phys., 11, 10791–10801, doi:10.5194/acp-11-10791-2011, 2011.

ACPD
14, 25825–25867, 2014

Laakso, L., Laakso, H., Aalto, P. P., Keronen, P., Petäjä, T., Nieminen, T., Pohja, T., Siivola, E., Kulmala, M., Kgabi, N., Molefe, M., Mabaso, D., Phalatse, D., Pienaar, K., and Kerminen, V.-M.: Basic characteristics of atmospheric particles, trace gases and meteorology in a relatively clean Southern African Savannah environment, Atmos. Chem. Phys., 8, 4823–4839, doi:10.5194/acp-8-4823-2008, 2008.

Laakso, L., Vakkari, V., Virkkula, A., Laakso, H., Backman, J., Kulmala, M., Beukes, J. P., van Zyl, P. G., Tiitta, P., Josipovic, M., Pienaar, J. J., Chiloane, K., Gilardoni, S., Vignati, E., Wiedensohler, A., Tuch, T., Birmili, W., Piketh, S., Collett, K., Fourie, G. D., Komppula, M., Lihavainen, H., de Leeuw, G., and Kerminen, V.-M.: South African EUCAARI measurements: seasonal variation of trace gases and aerosol optical properties, Atmos. Chem. Phys., 12, 1847–1864, doi:10.5194/acp-12-1847-2012, 2012.

Lee, K. H., Li, Z., Kim, Y. J., and Kokhanovsky, A.: Atmospheric aerosol monitoring from satellite observations: a history of three decades. In Atmospheric and biological environmental monitoring, Springer Netherlands, 2009.

Lehtinen, K. E. J., Korhonen, H., Dal Maso, M., and Kulmala, M.: On the concept of condensation sink diameter, Boreal Environ. Res., 8, 405–411, 2003.

Levy, R. C., Mattoo, S., Munchak, L. A., Remer, L. A., Sayer, A. M., Patadia, F., and Hsu, N. C.: The Collection 6 MODIS aerosol products over land and ocean, Atmos. Meas. Tech., 6, 2989–3034, doi:10.5194/amt-6-2989-2013, 2013.

Lourens, A. S. M., Beukes, J. P., Van Zyl, P. G., Fourie, G. D., Burger, J. W., Pienaar, J. J., Read, C. E., and Jordaan, J. H.: Spatial and Temporal assessment of gaseous pollutants in the Highveld of South Africa, S. Afr. J. Sci., 107, doi:10.4102/sajs.v107i1/2.269, 2011.

Lourens, A. S. M., Butler, T. M., Beukes, J. P., Van Zyl, P. G., Beirle, S., Wagner, T., Heue, K- P., Pienaar, J. J., Fourie, G. D., and Lawrence, M. G.: Re-evaluating the NO_2 hotspot over the South African Highveld, S. Afr. J. Sci., 108, 1146, doi:10.4102/sajs.v108i11/12.1146, 2012.

Maritz, P., Beukes, J. P., Van Zyl, P. G., Conradie, E. H., Liousse, C., Galy-Lacaux, C., Castéra, P., Ramandh, A., Mkhatshwa, G., Venter, A. D., and Pienaar, J. J.: Spatial and temporal assessment of organic and black carbon at IDAF sites in South Africa, Environ. Monit. Assess., submitted, 2014.

Mielonen, T., Levy, R. C., Aaltonen, V., Komppula, M., de Leeuw, G., Huttunen, J., Lihavainen, H., Kolmonen, P., Lehtinen, K. E. J., and Arola, A.: Evaluating the assumptions of surface reflectance and aerosol type selection within the MODIS aerosol retrieval over

ACPD
14, 25825–25867, 2014

land: the problem of dust type selection, Atmos. Meas. Tech., 4, 201–214, doi:10.5194/amt-4-201-2011, 2011.
Mishchenko, M. I., Travis, L. D., and Lacis, A. A.: Scattering, Absorption, and Emission of Light by Small Particles, Cambridge University Press, Cambridge, 2002.
Petäjä, T., Mauldin III, R. L., Kosciuch, E., McGrath, J., Nieminen, T., Paasonen, P., Boy, M., Adamov, A., Kotiaho, T., and Kulmala, M.: Sulfuric acid and OH concentrations in a boreal forest site, Atmos. Chem. Phys., 9, 7435–7448, doi:10.5194/acp-9-7435-2009, 2009.
Petäjä, T., Vakkari, V., Pohja, T., Nieminen, T., Laakso, H., Aalto, P. P., Keronen, P., Siivola, E., Kerminen, V.-M., Kulmala, M., and Laakso, L.: Transportable aerosol characterization trailer with trace gas chemistry: design, instruments and verification, Aerosol Air Qual. Res., 13, 421–435, 2013.
Schnelle-Kreis, J., Küpper, U., Sklorz, M., Cyrys, J., Briedé, J. J., Peters, A., and Zimmerman, R.: Daily measurements of organic compounds in ambient particulate matter in Augsburg, Germany: new aspects on aerosol sources and aerosol related health effects, Biomarkers, 14, 39–44, 2009.
Seaton, A., MacNee, W., Donaldson, K., and Godden, D.: Particulate air pollution and acute health effects, Lancet, 345, 176–178, 1995.
Shi, Y., Zhang, J., Reid, J. S., Hyer, E. J., and Hsu, N. C.: Critical evaluation of the MODIS Deep Blue aerosol optical depth product for data assimilation over North Africa, Atmos. Meas. Tech., 6, 949–969, doi:10.5194/amt-6-949-2013, 2013.
Tanskanen, A., Krotkov, N. A., J. R. Herman, and Arola, A.: Surface ultraviolet irradiance from OMI, IEEE T. Geosci. Remote, 44, 1267–1271, 2006.
Utell, M. J. and Frampton, M. W.: Acute health effects of ambient air pollution: the ultrafine particle hypothesis, J. Aerosol Med. Pulm. D., 13, 355–359, 2000.
Vakkari, V., Laakso, H., Kulmala, M., Laaksonen, A., Mabaso, D., Molefe, M., Kgabi, N., and Laakso, L.: New particle formation events in semi-clean South African savannah, Atmos. Chem. Phys., 11, 3333–3346, doi:10.5194/acp-11-3333-2011, 2011.
Vakkari, V., Beukes, J. P., Laakso, H., Mabaso, D., Pienaar, J. J., Kulmala, M., and Laakso, L.: Long-term observations of aerosol size distributions in semi-clean and polluted savannah in South Africa, Atmos. Chem. Phys., 13, 1751–1770, doi:10.5194/acp-13-1751-2013, 2013.
Veefkind, J. P., Boersma, K. F., Wang, J., Kurosu, T. P., Krotkov, N., Chance, K., and Levelt, P. F.: Global satellite analysis of the relation between aerosols and short-lived trace gases, Atmos. Chem. Phys., 11, 1255–1267, doi:10.5194/acp-11-1255-2011, 2011.

ACPD
14, 25825–25867, 2014

Venter, A. D., Vakkari, V., Beukes, J. P., van Zyl, P. G., Laakso, H., Mabaso, D., Tiitta, P., Josipovic, M., Kulmala, M., Pienaar, J. J., and Laakso. L.: An air quality assessment in the industrialised western Bushveld Igneous Complex, South Africa, S. Afr. J. Sci., 108, 1059, doi:10.4102/sajs.v108i9/10.1059, 2012.

Virkkula, A., Backman, J., Aalto, P. P., Hulkkonen, M., Riuttanen, L., Nieminen, T., dal Maso, M., Sogacheva, L., de Leeuw, G., and Kulmala, M.: Seasonal cycle, size dependencies, and source analyses of aerosol optical properties at the SMEAR II measurement station in Hyytiälä, Finland, Atmos. Chem. Phys., 11, 4445–4468, doi:10.5194/acp-11-4445-2011, 2011.

Winker, D. M., Hunt, W. M., and McGill, M. J.: Initial performance assessment of CALIOP, Geophys. Res. Lett., 34, L19803, doi:10.1029/2007GL030135, 2007.

York, D., Evensen, N., Martinez, M., and Delgado, J.: Unified equations for the slope, intercept, and standard errors of the best straight line, Am. J. Phys., 72, 367–375, 2004.

ACPD
14, 25825–25867, 2014

Table 1. A summary of the measurements used in this study. Here are listed only measurements between the study period 1 January 2007–31 December 2010.

Instrument	Measurement area/ Location	Measurement period	Measured parameters
Ozone Monitoring instrument OMI (satellite)	25.0–28.0° S, 25.5–30.5° E (whole study area)	Jan 2007–Dec 2010, obs. appr. once/day, only cloud-free obs.	NO_2 and SO_2 column densities, UV-B irradiance
Moderate Imaging Spectroradiometer MODIS (Aqua, satellite)	25.0–28.0° S, 25.5–30.5° E (whole study area)	Jan 2007–Dec 2010, obs. appr. once/day, only cloud-free obs.	Column integrated aerosol optical depth AOD at 550 nm wavelength
Cloud–Aerosol Lidar with Orthogonal Polarization CALIOP (satellite based lidar)	Selected locations within the study area	Selected days between Jan 2007–Dec 2010	Vertical profile of aerosol extinction at 532 nm waelength
Aerosol Robotic Network AERONET Sunphotometer (in situ)	Elandsfontein (26.25° S, 29.42° E)	Mar–Dec 2010, only cloudfree obs. during daylight.	Column integrated aerosol optical depth AOD at 500 nm wavelength.
Nephelometer (in situ)	Elandsfontein	Mar–Dec 2010	Aerosol scattering coefficient
Differential Mobility Particle Sizer DMPS (in situ)	Marikana (25.70° S, 27.48° E) Botsalano (25.54° S, 25.75° E) Welgegund (26.57° S, 26.94° E)	Marikana: Feb 2008–May 2010 Botsalano: Jan 2007–Feb 2008 Welgegund: May–Dec 2010	Particle size distribution, condensation sink, event classification
Scanning Mobility Particle Sizer SMPS (in situ)	Elandsfontein	Mar–Dec 2010	Particle size distribution, condensation sink
	All in situ stations	dates/station as above	NO_x, and NO, SO_2, global radiation, T, RH

ACPD
14, 25825–25867, 2014

Table 2. Correlations between in situ and satellite based proxies.

Station	$(NO_x\text{-}NO)/CS$ vs. NO_2/AOD	SO_2/CS vs. SO_2/AOD	$SO_2 \cdot UV\text{-}B/cs^2$ vs. $SO_2 \cdot UV\text{-}B/AOD^2$	$Glob./CS^2$ vs. $UV\text{-}B/AOD^2$
Elandsfontein	$R = 0.33$ ($p = 0.026$)	$R = 0.20$ ($p = 0.218$)	$R = 0.19$ ($p = 0.236$)	$R = 0.31$ ($p = 0.051$)
Marikana	$R = 0.62$ ($p < 0.001$)	$R = 0.07$ ($p = 0.554$)	$R = -0.04$ ($p = 0.700$)	$R = 0.41$ ($p < 0.001$)
Botsalano	$R = -0.06$ ($p = 0.821$)	$R = 0.35$ ($p = 0.225$)	$R = 0.29$ ($p = 0.309$)	$R = 0.62$, ($p = 0.017$)

ACPD
14, 25825–25867, 2014

Table 3. Correlation between the satellite-based proxies and number concentration of nucleation mode particles ($D_p < 30$ nm) at Marikana measurement station. The first column presents the correlations when AOD is used to estimate the sink due to pre-existing aerosols, and the second column represents the correlations when the sink is estimated using the York fit for coincident CS-AOD observations shown in Fig. 5.

Proxy	Sink = AOD	Sink = 0.172 · AOD – 0.008
NO_2/Sink	$R = 0.31$ ($p < 0.001$)	$R = 0.34$ ($p < 0.001$)
SO_2/Sink	$R = 0.11$ ($p = 0.313$)	$R = 0.23$ ($p = 0.046$)
$SO_2 \cdot$ UV-B/Sink^2	$R = 0.09$ ($p = 0.390$)	$R = 0.21$ ($p = 0.046$)
UV-B/Sink^2	$R = 0.17$ ($p = 0.067$)	$R = 0.25$ ($p = 0.006$)

ACPD
14, 25825–25867, 2014

Table 4. A summary of the new particle formation event data at Marikana, Botsalano, and Welgegund stations. The table includes only the measurements that were available between January 2007–December 2010. In the brackets it is shown the percentages of days when the satellite proxies could be determined at the station (depending on which proxy was considered). In the most of the cases satellite based proxies could not be determined because of missing AOD due to cloudiness.

Station (measurement period)	Number of measurement days	Number of event days	Number of undefined days	Number of non-event days
Marikana (8 Feb 2008–17 May 2010)	659	568 (14–21 %)	89 (8–7 %)	2 (0 %)
Botsalano (1 Jan 2007–5 Feb 2008)	365	252 (4–5 %)	95 (4–5 %)	18 (0 %)
Welgegund (20 May–31 Dec 2010)	118	93 (6–3 %)	24 (8–4 %)	1 (0 %)

ACPD
14, 25825–25867, 2014

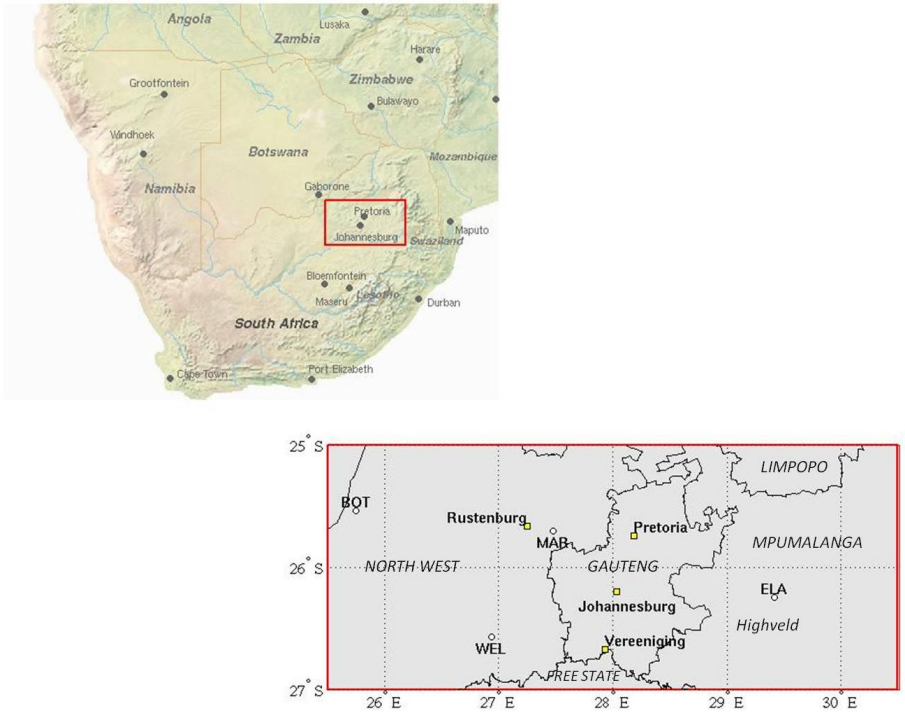

Figure 1. The study area and locations of the in situ measurement stations; BOT = Botsalano, MAR = Marikana, WEL = Welgegund, and ELA = Elandsfontein.

ACPD
14, 25825–25867, 2014

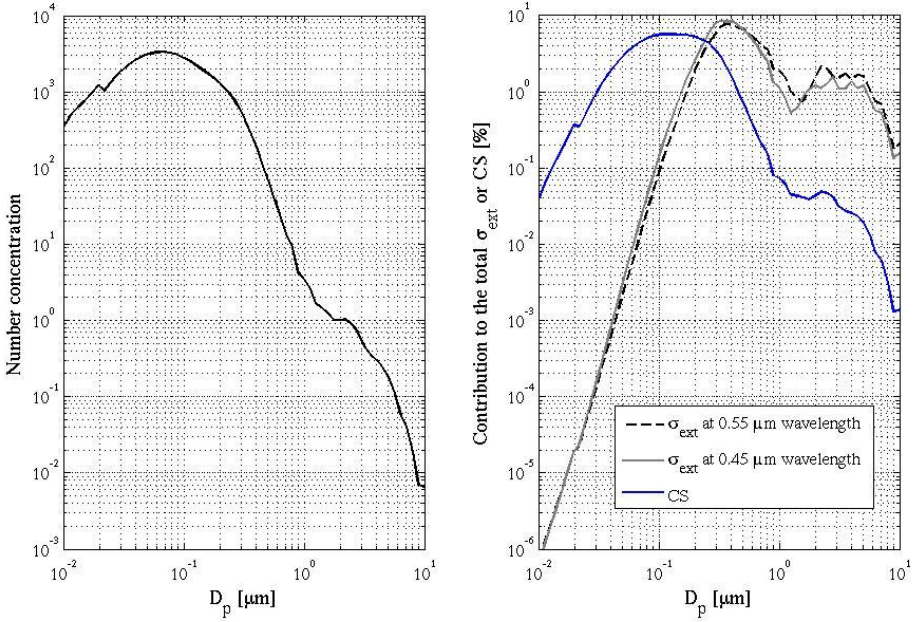

Figure 2. The sensitivity of CS and aerosol extinction coefficient to different particle sizes. In the left panel is shown the aerosol size distribution that is used to calculate CS and rho_ext. In the right panel is shown the contribution of each particle size to the total CS and rho_ext. The σ_{ext} is calculated for two wavelengths (0.55 and 0.45 μm) assuming spherical particles with a refractive index of $m = 1.48 + 0.001i$.

ACPD
14, 25825–25867, 2014

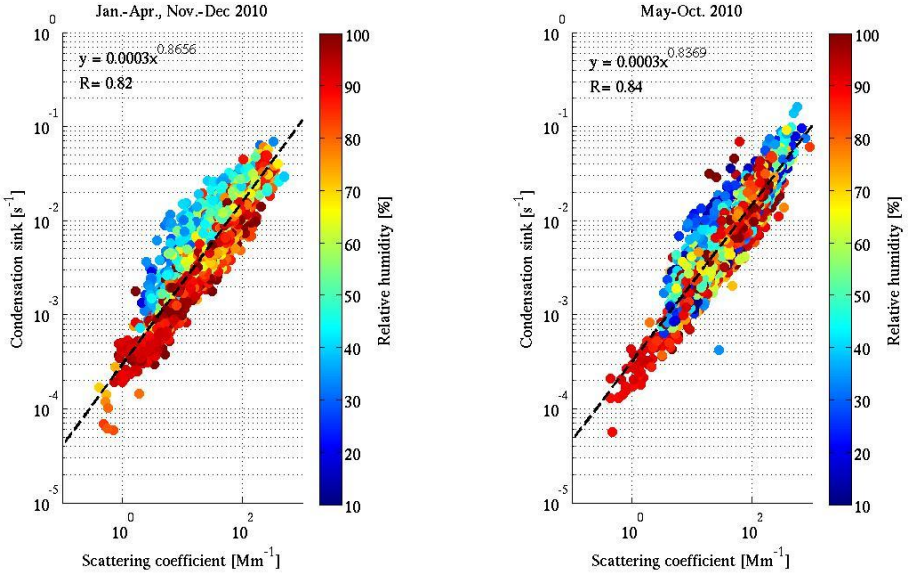

Figure 3. The comparison between in situ condensation sink and nephelometer scattering coefficient at Elandsfontein measurement station in 2010 for warm (January–April, November–December), and cold season (May–October). CS has been corrected to the ambient relative humidity but the scattering coefficient represents scattering from dry particles.

ACPD
14, 25825–25867, 2014

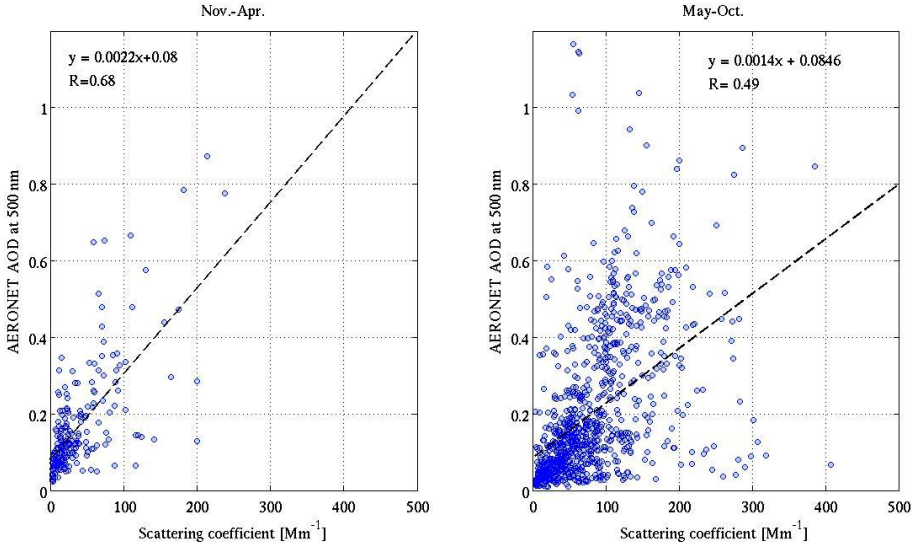

Figure 4. Comparison between the AERONET AOD and in situ scattering coefficient at Elandsfontein measurement station. The AOD is the column integrated value of aerosol extinction (scattering + absorption) obtained from the sunphotometer measurements. The in situ scattering coefficient is obtained from the nephelometer.

ACPD
14, 25825–25867, 2014

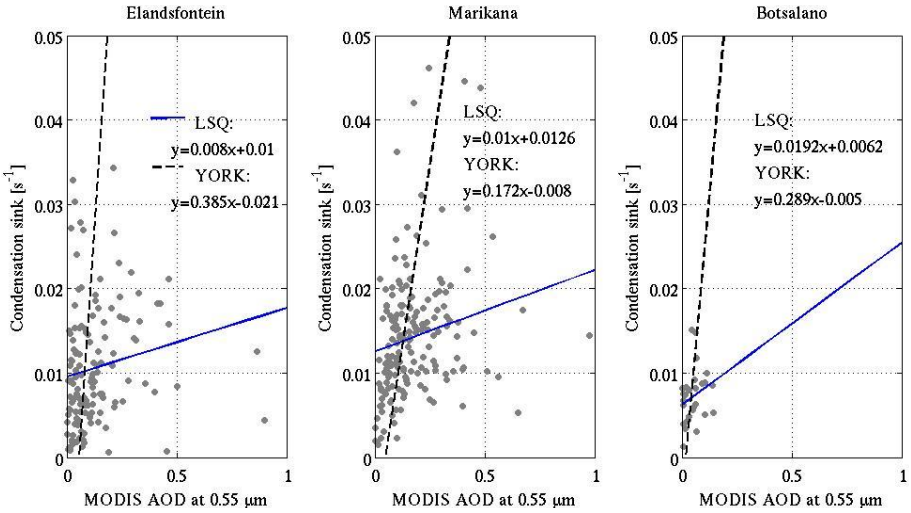

Figure 5. Comparison between MODIS AOD and in situ CS. The MODIS AOD values are spatial averages calculated from the observations within 3 km distance from the measurement station, whereas the CS values are one hour averages (13:00–14:00 LT). The blue lines represent the slope from least squares linear fitting (LSQ). The correlation coefficients for Elandsfontein, Marikana, and Botsalano were $R = 0.17$ ($p = 0.054$), $R = 0.23$, ($p = 0.002$), and $R = 0.25$ ($p = 0.201$), respectively. The dashed black lines represent the fitting method where the uncertainties related to CS and AOD values have been taken into account (YORK, York et al., 2004). The uncertainty for CS was set to 10 %, and for AOD to 0.05 + 15 % (Levy et al., 2013).

ACPD
14, 25825–25867, 2014

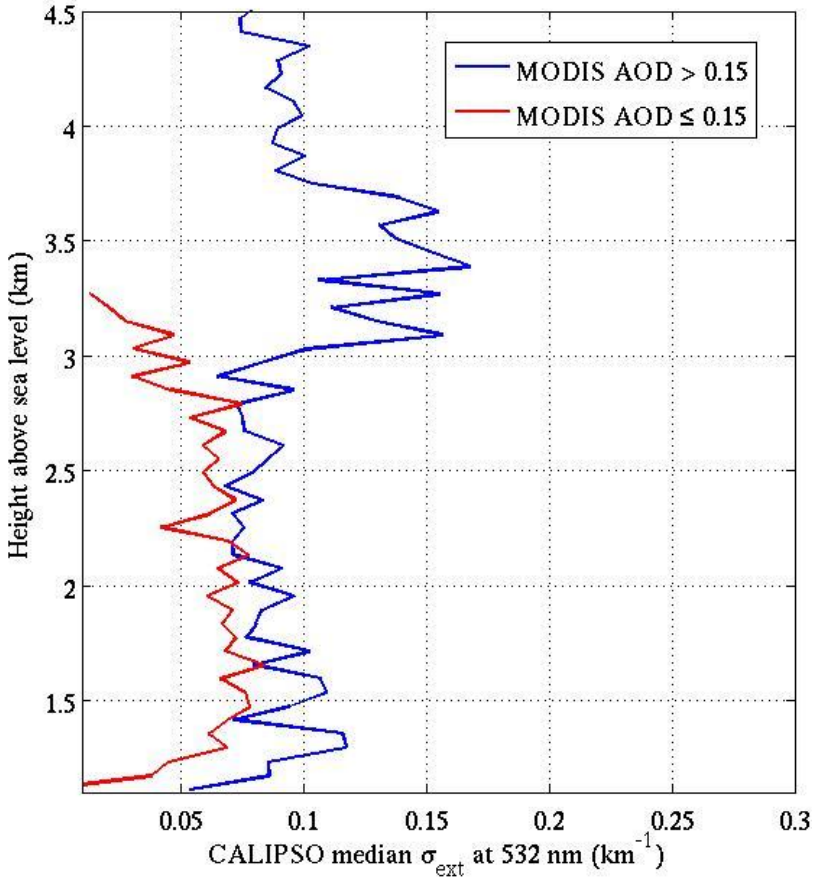

Figure 6. Median CALIPSO extinction profiles for days when MODIS AOD was greater (blue) and lower (red) than the measurement period median (0.15). The CALIPSO profiles are collected within 50 km radius from the Marikana station.

ACPD
14, 25825–25867, 2014

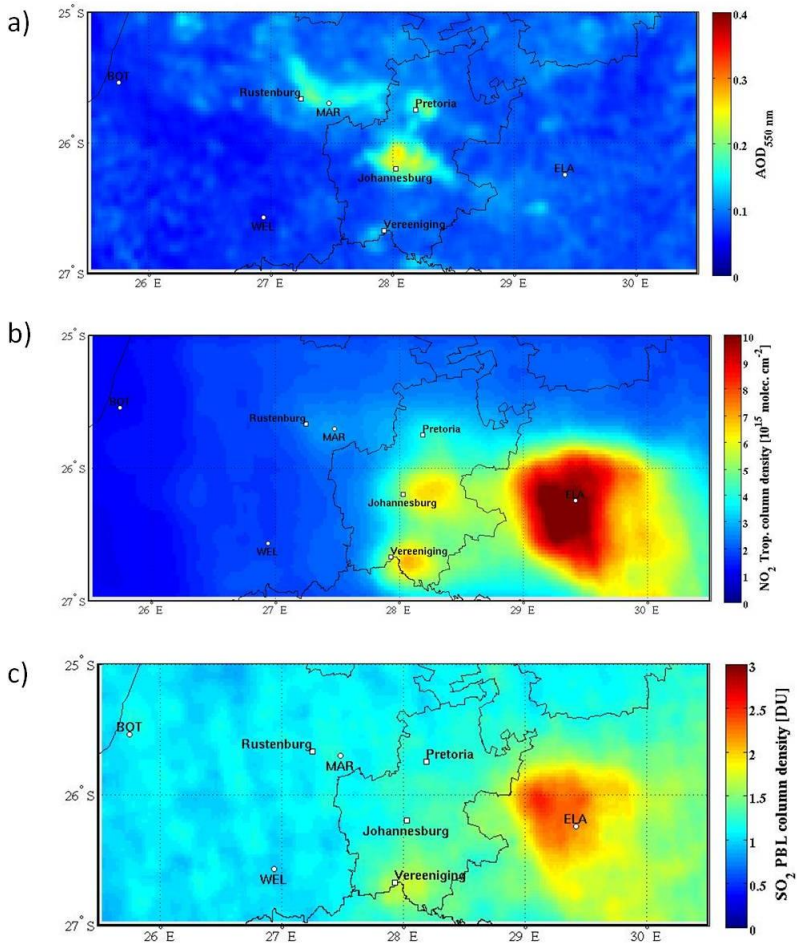

Figure 7. MODIS AOD **(a)**, OMI NO_2 **(b)** and SO_2 **(c)** column density medians for a four year period from January 2007 to December 2010.

ACPD
14, 25825–25867, 2014

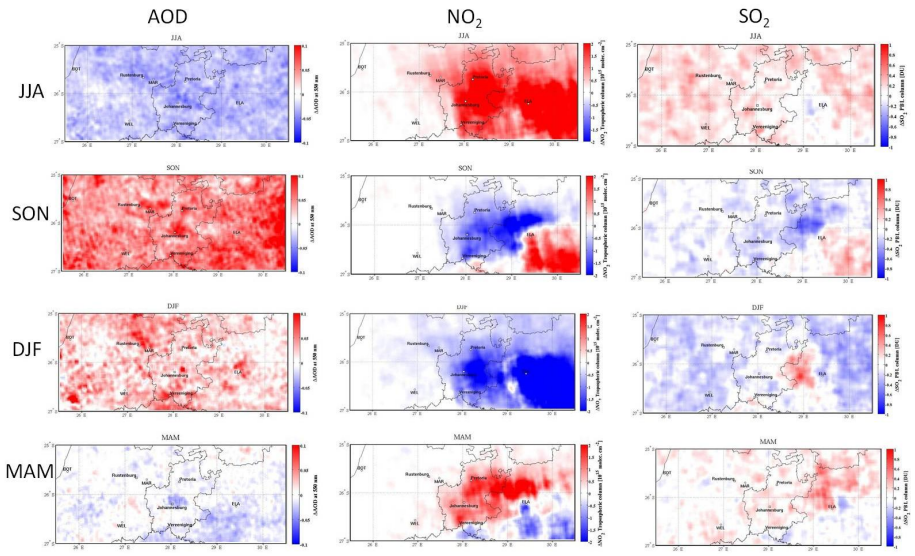

Figure 8. Seasonal anomalies of MODIS AOD (left panel), OMI NO_2 (middle panel) and SO_2 (right panel) column densities. The anomalies are calculated using data between January 2007–December 2010.

ACPD
14, 25825–25867, 2014

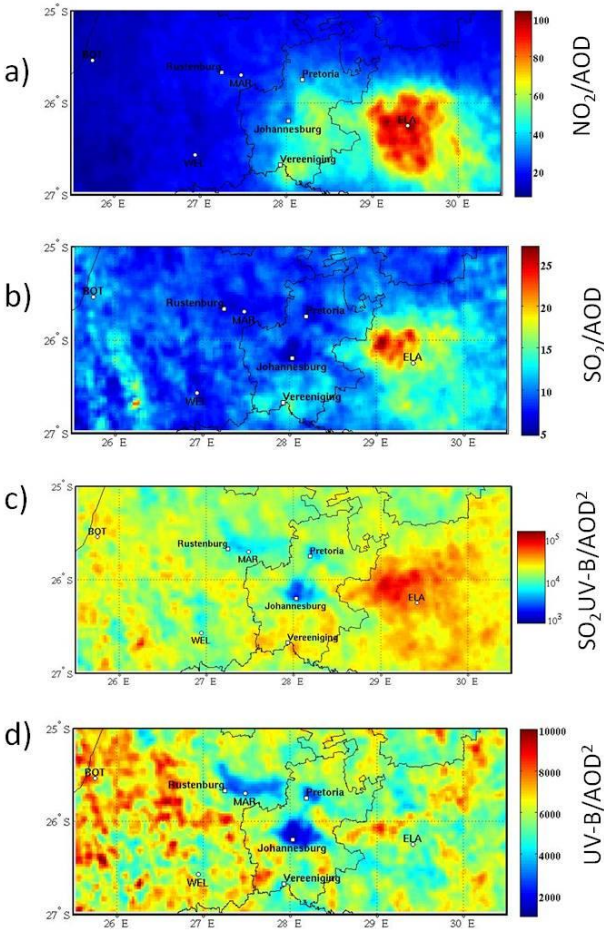

Figure 9. Satellite based proxy medians for 2007–2010 for **(a)** NO_2/AOD, **(b)** SO_2/AOD, **(c)** $SO_2 \cdot$UV-B/AOD^2, and **(d)** UV-B/AOD^2.

ACPD
14, 25825–25867, 2014

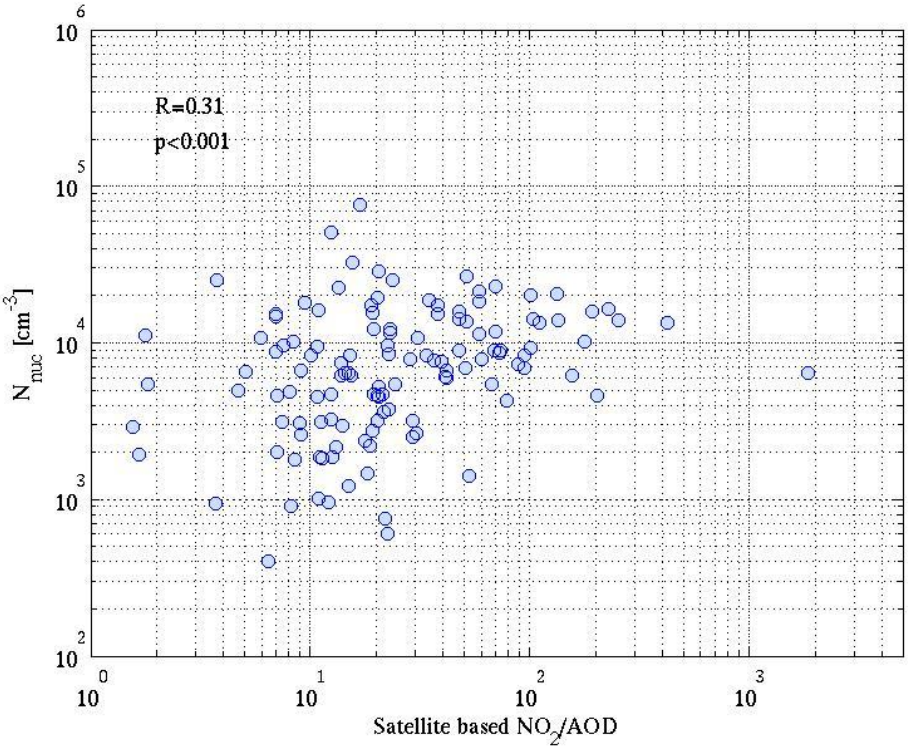

Figure 10. The comparison between the number concentration of nucleation mode (D < 30 nm) particles and satellite based proxy NO_2/AOD. The number concentrations are one hour averages (13:00–14:00 LT), whereas the satellite proxy value is about the satellite overpass at 13:30 LT.

ACPD
14, 25825–25867, 2014

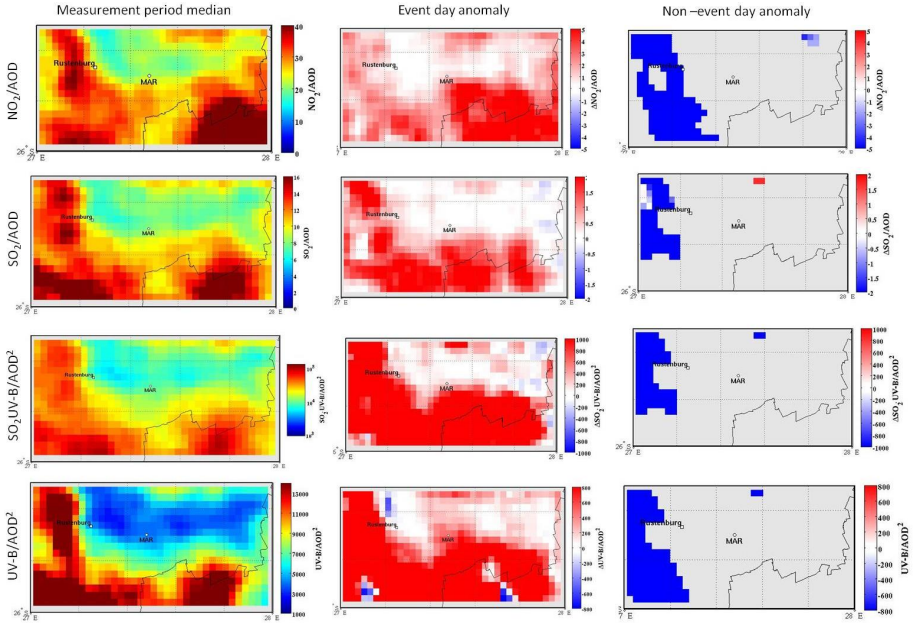

Figure 11. Satellite proxy medians, event-, and non-event-day anomalies calculated from the event classification data obtained at Marikana measurement station. The proxies considered were (starting from top row) NO_2/AOD, SO_2/AOD, $SO_2 \cdot$UV-B/AOD^2, and UV-B/AOD^2. The grey areas designate missing values. For the non-event days the proxy data was missing mainly due to cloudiness.

ACPD
14, 25825–25867, 2014

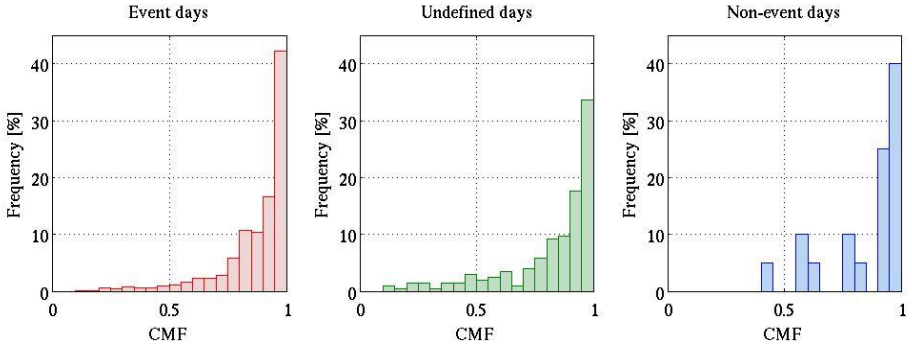

Figure 12. The OMI cloud modification factor (CMF) distribution for event, undefined and non-event days. The distributions are combined data from Marikana and Botsalano measurement stations. The number of event, undefined, and non-event day CMF observations were 768, 205, and 20 respectively.

ACPD
14, 25825–25867, 2014